Series Solutions for the Peristaltic Flow of a Tangent Hyperbolic Fluid in a Uniform Inclined Tube

Sohail Nadeem and Noreen Sher Akbar

Department of Mathematics, Quaid-i-Azam University 45320, Islamabad 44000, Pakistan

Reprint requests to S. N.; E-mail: snqau@hotmail.com

Z. Naturforsch. **65a,** 887 – 895 (2010); received June 4, 2009 / revised November 6, 2009

In the present investigation we have studied a tangent hyperbolic fluid in a uniform inclined tube. The governing equations are simplified using long wavelength and low Reynold number approximations. The solutions of the problem in simplified form are calculated with two methods namely (i) the perturbation method and (ii) the homotopy analysis method. The comparison of the solutions show a very good agreement between the two results. At the end of the article the expressions of the pressure rise and the frictional force are calculated with the help of numerical integration. The graphical results are presented to show the physical behaviour of Weissenberg number We, amplitude ratio ϕ, and tangent hyperbolic power law index n.

Key words: Series Solutions; Peristaltic Flow; Tangent Hyperbolic Fluid; Uniform Tube.

1. Introduction

The study of non-Newtonians fluids have become an increasing importance in the last few decades. This is mainly due to its large number of applications in many areas. Such applications are foodmixing and chyme movement in the intestine, flow of plasma, flow of blood, polymer fluids, colloidal suspension, liquid crystals, animal blood exotic lubricants, and fluid containing small additives. Another reason which has attracted the attention of various researcher's to discuss the non-Newtonian fluids is that an universal non-Newton constitutive relation that can be used for all fluids and flows is not available. Therefore, a number of studies have been presented which deal with different kinds of non-Newtonian fluid models using different kinds of geometries [1 – 6]. Peristaltic mechanism is also a rich of research area which has attracted the attention of researchers due to its wide range of applications in physiology and industry. After the first investigation done by Latham [7] a number of studies dealing with different flow geometries have been discussed in peristaltic flow problem [8 – 18].

In view of the above analysis the purpose of the present investigation is multidimensional. The main aim is to discuss the peristaltic flow of a tangent hyperbolic fluid model and the secondary purpose is to find the series solutions of nonlinear equations of the given problem with the help of the homotopy analysis method and the perturbation method. The governing equations of the problem are first simplified and then the reduced nonlinear equations are solved analytically. The expressions for the pressure rise and frictional forces are calculated numerically. The highlights of the problems are discussed through graphs.

2. Mathematical Model

For an incompressible fluid the balance of mass and momentum are given by

$$\operatorname{div}\mathbf{V} = 0, \tag{1}$$

$$\rho\frac{\mathrm{d}\mathbf{V}}{\mathrm{d}t} = \operatorname{div}\mathbf{S} + \rho\mathbf{f}, \tag{2}$$

where ρ is the density, $\mathbf{V}$ is the velocity vector, $\mathbf{S}$ is the Cauchy stress tensor, $\mathbf{f}$ represents the specific body force, and $\mathrm{d}/\mathrm{d}t$ represents the material time derivative. The constitutive equation for a hyperbolic tangent fluid is given by [5]

$$\mathbf{S} = -P\mathbf{I} + \boldsymbol{\tau}, \tag{3}$$

$$\boldsymbol{\tau} = \left[\left[\eta_\infty + (\eta_0 + \eta_\infty)\tanh(\Gamma\overline{\dot{\gamma}})^n\right]\overline{\dot{\gamma}}\right], \tag{4}$$

in which $-P\mathbf{I}$ is the spherical part of the stress due to constraint of incompressibility, $\boldsymbol{\tau}$ is the extra stress tensor, η_∞ is the infinite shear rate viscosity, η_0 is the

0932–0784 / 10 / 1100–0887 $ 06.00

zero shear rate viscosity, Γ is the time constant, n is the power law index, and $\bar{\dot{\gamma}}$ is defined as

$$\bar{\dot{\gamma}} = \sqrt{\frac{1}{2}\sum_i\sum_j \bar{\dot{\gamma}}_{ij}\bar{\dot{\gamma}}_{ji}} = \sqrt{\frac{1}{2}\Pi}, \tag{5}$$

where $\Pi = \frac{1}{2}\mathrm{tr}(\mathrm{grad}V + (\mathrm{grad}V)^T)^2$ is the second invariant strain tensor. We consider the constitution (4), the case for which $\eta_\infty = 0$ and $\Gamma\bar{\dot{\gamma}} < 1$. The component of extra stress tensor, therefore, can be written as

$$\begin{aligned}\bar{\boldsymbol{\tau}} &= \eta_0[(\Gamma\bar{\dot{\gamma}})^n]\bar{\dot{\gamma}} = \eta_0[(1+\Gamma\bar{\dot{\gamma}}-1)^n]\bar{\dot{\gamma}}\\ &= \eta_0[1+n(\Gamma\bar{\dot{\gamma}}-1)]\bar{\dot{\gamma}}.\end{aligned} \tag{6}$$

3. Mathematical Formulation

Let us consider the peristaltic transport of an incompressible hyperbolic tangent fluid in a two dimensional inclined tube. The flow is generated by sinusoidal wave trains propagating with constant speed c along the channel walls. The geometry of the wall surface is defined as

$$\bar{h} = a + b\sin\frac{2\pi}{\lambda}(\bar{Z} - c\bar{t}), \tag{7}$$

where a is the radius of the tube, b is the wave amplitude, λ is the wavelength, c is the propagation velocity, and $\bar{t}$ is the time. We are considering the cylindrical coordinate system $(\bar{R},\bar{Z})$, in which the $\bar{Z}$-axis lies along the centerline of the tube and $\bar{R}$ is transverse to it (see Fig. 1).

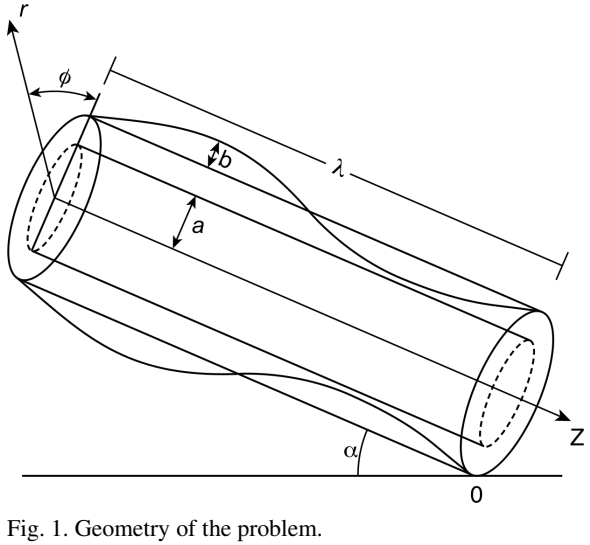

Fig. 1. Geometry of the problem.

The governing equations in the fixed frame for an incompressible flow are

$$\frac{\partial\bar{U}}{\partial\bar{R}} + \frac{\bar{U}}{\bar{R}} + \frac{\partial\bar{W}}{\partial\bar{Z}} = 0, \tag{8}$$

$$\begin{aligned}&\rho\left(\frac{\partial}{\partial\bar{t}} + \bar{U}\frac{\partial}{\partial\bar{R}} + \bar{W}\frac{\partial}{\partial\bar{Z}}\right)\bar{U} =\\ &-\frac{\partial\bar{P}}{\partial\bar{R}} + \frac{1}{\bar{R}}\frac{\partial}{\partial\bar{R}}(\bar{R}\bar{\boldsymbol{\tau}}_{\bar{R}\bar{R}}) + \frac{\partial}{\partial\bar{Z}}(\bar{\boldsymbol{\tau}}_{\bar{R}\bar{Z}}) + \frac{\bar{\boldsymbol{\tau}}_{\bar{\theta}\bar{\theta}}}{\bar{R}},\end{aligned} \tag{9}$$

$$\begin{aligned}&\rho\left(\frac{\partial}{\partial\bar{t}} + \bar{U}\frac{\partial}{\partial\bar{R}} + \bar{W}\frac{\partial}{\partial\bar{Z}}\right)\bar{W} =\\ &-\frac{\partial\bar{P}}{\partial\bar{Z}} + \frac{1}{\bar{R}}\frac{\partial}{\partial\bar{R}}(\bar{R}\bar{\boldsymbol{\tau}}_{\bar{R}\bar{Z}}) + \frac{\partial}{\partial\bar{Z}}(\bar{\boldsymbol{\tau}}_{\bar{Z}\bar{Z}}) - \rho g\sin\alpha.\end{aligned} \tag{10}$$

Introducing a wave frame $(\bar{r},\bar{z})$ moving with velocity c away from the fixed frame $(\bar{R},\bar{Z})$ by the transformations

$$\bar{z} = \bar{Z} - c\bar{t}, \quad \bar{r} = \bar{R}, \tag{11}$$

$$\bar{w} = \bar{W} - c, \quad \bar{u} = \bar{U}, \tag{12}$$

where $\bar{U},\bar{W}$ and $\bar{u},\bar{w}$ are the velocity components in the radial and axial directions in the fixed and moving coordinates, respectively.

The corresponding boundary conditions are

$$\frac{\partial\bar{w}}{\partial\bar{r}} = 0,\ \bar{u} = 0 \ \text{ at } \ \bar{r} = 0, \tag{12a}$$

$$\begin{aligned}&\bar{w} = -c,\ \bar{u} = -c\frac{\mathrm{d}\bar{h}}{\mathrm{d}\bar{z}}\\ &\text{at } \ \bar{r} = \bar{h} = a + b\sin\frac{2\pi}{\lambda}(\bar{z}).\end{aligned} \tag{12b}$$

Defining

$$\begin{aligned}&R = \frac{\bar{R}}{a}, \quad r = \frac{\bar{r}}{a}, \quad Z = \frac{\bar{Z}}{\lambda}, \quad z = \frac{\bar{z}}{\lambda},\\ &W = \frac{\bar{W}}{c}, \quad w = \frac{\bar{w}}{c}, \quad \boldsymbol{\tau} = \frac{a\bar{\boldsymbol{\tau}}}{c\mu}, \quad U = \frac{\lambda\bar{U}}{ac},\\ &u = \frac{\lambda\bar{u}}{ac}, \quad P = \frac{a^2\bar{P}}{c\lambda\mu}, \quad t = \frac{c\bar{t}}{\lambda}, \quad \delta = \frac{a}{\lambda},\\ &Re = \frac{\rho ca}{\mu}, \quad h = \frac{\bar{h}}{a} = 1 + \phi\sin 2\pi z,\\ &\dot{\gamma} = \frac{a}{c}\bar{\dot{\gamma}}, \quad E = \frac{\mu c}{\rho g a^2},\end{aligned} \tag{13}$$

where μ is the viscosity of the fluid.

Using the above non-dimensional quantities and the resulting equations can be written as

$$\frac{\partial u}{\partial r}+\frac{u}{r}+\frac{\partial w}{\partial z}=0, \tag{14}$$

$$Re\,\delta^3\left(u\frac{\partial}{\partial r}+w\frac{\partial}{\partial z}\right)u= -\frac{\partial P}{\partial r}-\frac{\delta}{r}\frac{\partial}{\partial r}(r\boldsymbol{\tau}_{rr})-\delta^2\frac{\partial}{\partial z}(\boldsymbol{\tau}_{rz}), \tag{15}$$

$$Re\,\delta\left(u\frac{\partial}{\partial r}+w\frac{\partial}{\partial z}\right)w= -\frac{\partial P}{\partial z}-\frac{1}{r}\frac{\partial}{\partial r}(r\boldsymbol{\tau}_{rz})-\delta\frac{\partial}{\partial z}(\boldsymbol{\tau}_{zz})-\frac{\sin\alpha}{E}, \tag{16}$$

where

$$\begin{aligned}\boldsymbol{\tau}_{rr}&=-2[1+n(We\dot{\gamma}-1)]\frac{\partial u}{\partial r},\\ \boldsymbol{\tau}_{rz}&=-[1+n(We\dot{\gamma}-1)]\left(\frac{\partial u}{\partial z}\delta^2+\frac{\partial w}{\partial r}\right),\\ \boldsymbol{\tau}_{zz}&=-2\delta[1+n(We\dot{\gamma}-1)]\frac{\partial w}{\partial z},\\ \dot{\gamma}&=\left[2\delta^2\left(\frac{\partial u}{\partial r}\right)^2+\left(\frac{\partial u}{\partial z}\delta^2+\frac{\partial w}{\partial r}\right)^2+2\delta^2\left(\frac{\partial w}{\partial z}\right)^2\right]^{1/2},\end{aligned} \tag{17}$$

in which δ, Re, We represent the wave, Reynolds, and Weissenberg numbers, respectively. Under the assumptions of long wavelength $\delta \ll 1$ and low Reynolds number, neglecting the terms of order δ and higher, (12), (15), and (16) take the form

$$\frac{\partial P}{\partial z}+\frac{\sin\alpha}{E}= \frac{1}{r}\frac{\partial}{\partial r}\left[r\left(1+n\left(We\frac{\partial w}{\partial r}-1\right)\right)\frac{\partial w}{\partial r}\right], \tag{18}$$

$$\frac{\partial P}{\partial r}=0, \tag{19}$$

$$\begin{aligned}&\frac{\partial w}{\partial r}=0, \text{ at } r=0,\\ &w=-1, \text{ at } r=h=1+\phi\sin 2\pi z.\end{aligned} \tag{20}$$

4. Solution of the Problem

4.1. Perturbation Solution

For perturbation solution, we expand w, F, and P as

$$w=w_0+Wew_1+O(We^2), \tag{21}$$

$$F=F_0+WeF_1+O(We^2), \tag{22}$$

$$P=P_0+WeP_1+O(We^2). \tag{23}$$

Expressions for velocity profile and pressure gradient satisfying the boundary conditions (20) can be written as

$$w=-1+\left(\frac{r^2-h^2}{4(1-n)}\right)\frac{\partial P}{\partial z}+\frac{\sin\alpha}{E}\frac{r^2-h^2}{4(1-n)} +We(a_{11}(r^3-h^3)), \tag{24}$$

$$\frac{\mathrm{d}P}{\mathrm{d}z}=\frac{-8E(1-n)(2F+h^2)-h^2\sin\alpha}{Eh^4} +We\left(-\frac{12}{5}a_{11}h\right). \tag{25}$$

4.2. Homotopy Analysis Method (HAM) Solution

In this section, we have found the HAM solution of (18) to (20). For that we choose

$$w_0=-1+\left(\frac{r^2-h^2}{4(1-n)}\right)\frac{\partial P}{\partial z}+\frac{\sin\alpha}{E}\frac{r^2-h^2}{4(1-n)}, \tag{26}$$

as the initial guess. Further, the auxiliary linear operator for the problem is taken as

$$\mathcal{L}_{wr}(w)=\frac{1}{r}\frac{\partial}{\partial r}\left(r\frac{\partial w_0}{\partial r}\right), \tag{27}$$

which satisfies

$$\mathcal{L}_{wr}(w_0)=0. \tag{28}$$

From (18) to (20) we can define the following zeroth-order deformation problems:

$$(1-q)\mathcal{L}_{wr}[\,\bar{w}(r,q)-w_0(r)]=q\hbar_w N_{wr}[\bar{w}(r,q)], \tag{29}$$

$$\begin{aligned}&\frac{\partial\bar{w}(r,q)}{\partial r}=0, \text{ at } r=0,\\ &\bar{w}(r,q)=-1, \text{ at } r=h.\end{aligned} \tag{30}$$

In (29) and (30), $\hbar_w$ denote the non-zero auxiliary parameter, $q\in[0,1]$ is the embedding parameter and

$$N_{wr}[\bar{w}(r,q)]=(1-n)\frac{\partial^2 w}{\partial r^2}+\frac{(1-n)}{r}\frac{\partial w}{\partial r} +\frac{nWe}{r}\left(\frac{\partial w}{\partial r}\right)^2+2nWe\frac{\partial^2 w}{\partial r^2}\frac{\partial w}{\partial r}-\frac{\mathrm{d}P}{\mathrm{d}z}. \tag{31}$$

Obviously,

$$\frac{\partial \hat{w}(r,0)}{\partial r} = w_0, \quad \hat{w}(r,1) = w(r), \tag{32}$$

when q varies from 0 to 1, then $\hat{w}(r,q)$ varies from initial guess to the solution $w(r)$. Expanding $\hat{w}(r,q)$ in Taylor series with respect to an embedding parameter q, we have

$$\hat{w}(r,q) = w_0(r) + \sum_{n=1}^{\infty} w_m(r) q^m, \tag{33}$$

$$w_m = \frac{1}{m!} \left. \frac{\partial^m \bar{w}(r,q)}{\partial q^m} \right|_{q=0}. \tag{34}$$

Differentiating the zeroth-order deformation m-times with respect to q and then dividing by $m!$ and finally setting $q = 0$, we get the following mth-order deformation problem:

$$\mathcal{L}_w[w_m(r) - \chi_m w_{m-1}(r)] = \hbar_w R_{wr}(r), \tag{35}$$

where

$$\begin{aligned} R_{wr} = {} & (1-n) w''_{m-1} + \frac{1}{r}(1-n) w'_{m-1} \\ & + \frac{nWe}{r} \sum_{i=0}^{m-1} w'_{m-1-k} w'_k \\ & + 2nWe \sum_{k=0}^{m-1} w'_{m-1-k} w''_k - \frac{\mathrm{d}P}{\mathrm{d}z}(1-\chi_m). \end{aligned} \tag{36}$$

$$\chi_m = \begin{cases} 0, & m \le 1, \\ 1, & m > 1. \end{cases} \tag{37}$$

The solution of the above equation with the help of Mathematica can be calculated and presented as follows:

$$\begin{aligned} w_m(r) = \lim_{M \to \infty} \Bigg[& \sum_{m=0}^{M} a^0_{m,0} \\ & + \sum_{n=1}^{2M+1} \left(\sum_{m=n-1}^{2M} \sum_{k=1}^{2m+1-n} a^k_{m,n} r^{n+2} \right) \Bigg], \end{aligned} \tag{38}$$

where $a^0_{m,0}$ and $a^k_{m,n}$ are constants.

5. Graphical Results and Discussion

In this section the pressure rise, frictional forces, and axial pressure gradient are discussed carefully and

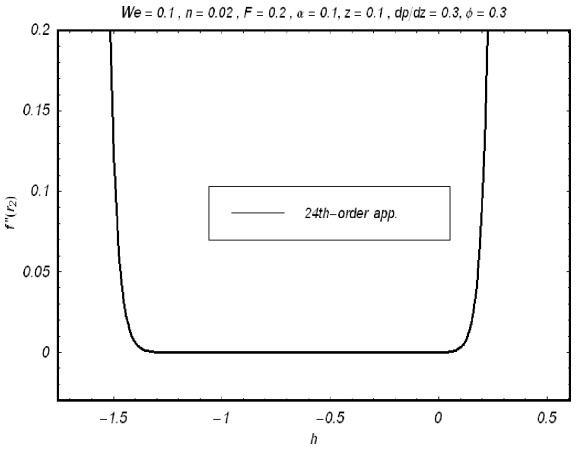

Fig. 2. h-curve for the velocity field.

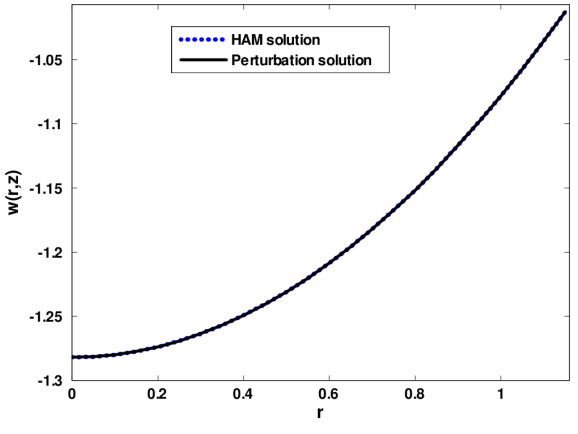

Fig. 3. Comparison of velocity field for $We = 0.1$, $\alpha = 0.1$, $\phi = 0.3$, $z = 0.1$, $\mathrm{d}P/\mathrm{d}z = 0.8$, $n = 0.4$, $E = 15$, and $h = -1$.

shown graphically (see Figs. 4 to 15). The pressure rise is calculated numerically by using Mathematica. Figures 4 to 7 show the pressure rise ΔP against the volume flow rate Θ for different values of angle of inclination α, Weissenberg number We, amplitude ratio ϕ, and tangent hyperbolic power law index n. These figures indicate that the relation between pressure rise and volume flow rate are inversely proportional to each other. It is observed from Figure 4 that with the increase in α, pressure rise increases. It is analyzed that through Figures 5 and 6 that with an increase in n and We, pressure rise increases for $0 \le \Theta \le 0.3$, while decreases for $0.31 \le \Theta \le 1$. Figure 7 show that with an increase in ϕ the pressure rise decreases for $0 \le \Theta \le 0.5$ while increases for $0.51 \le \Theta \le 1$. Peristaltic pumping occurs in the region $0 \le \Theta \le 0.3$ for Figures 5 and 6, $0 \le \Theta \le 0.5$ for Figure 7, otherwise

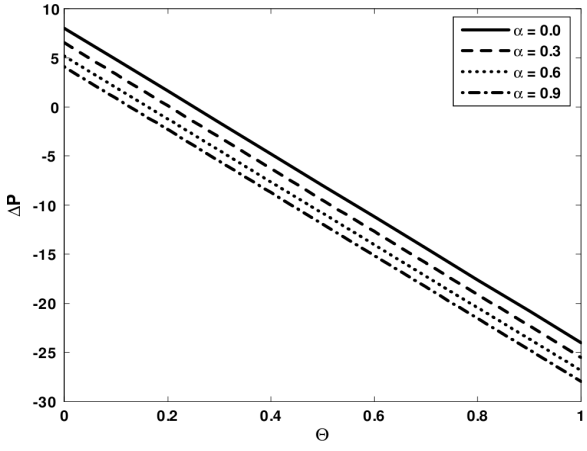

Fig. 4. Pressure rise versus flow rate for $We = 0.1$, $n = 0.02$, $\phi = 0.01$, and $E = 0.2$.

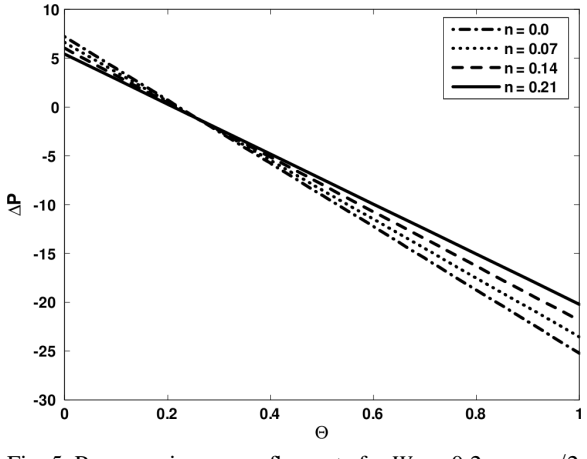

Fig. 5. Pressure rise versus flow rate for $We = 0.2$, $\alpha = \pi/2$, $\phi = 0.05$, and $E = 1$.

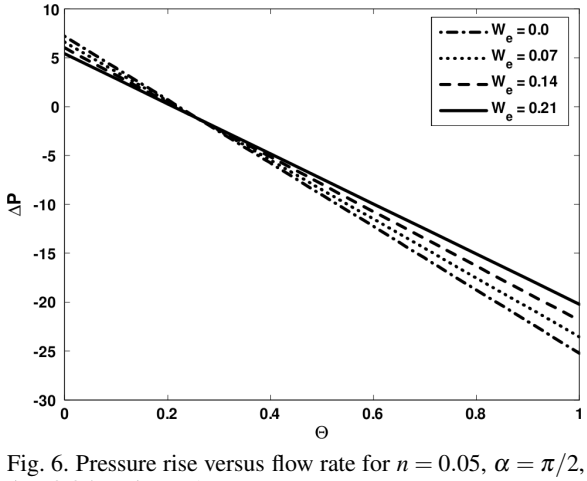

Fig. 6. Pressure rise versus flow rate for $n = 0.05$, $\alpha = \pi/2$, $\phi = 0.05$, and $E = 1$.

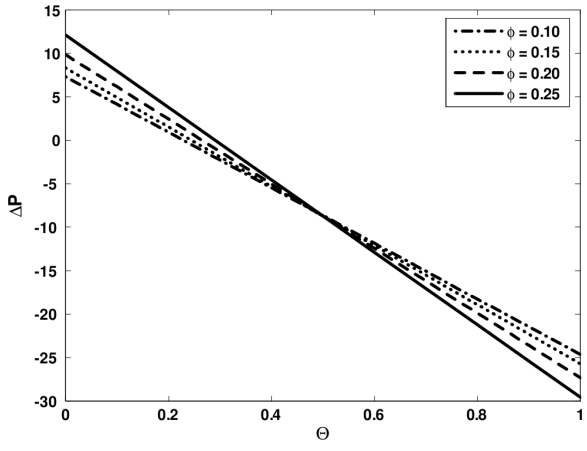

Fig. 7. Pressure rise versus flow rate for $n = 0.05$, $\alpha = \pi/2$, $We = 0.2$, and $E = 1$.

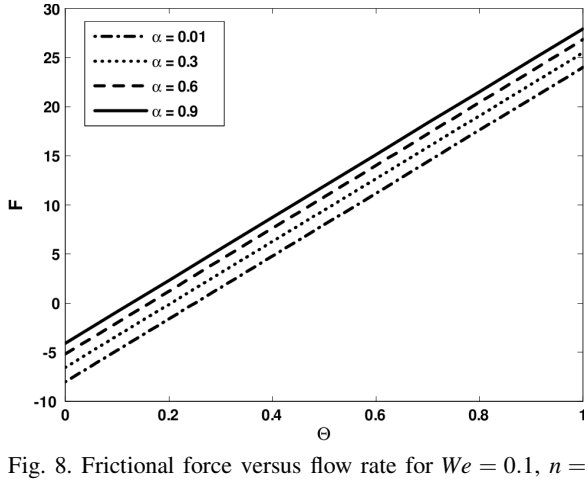

Fig. 8. Frictional force versus flow rate for $We = 0.1$, $n = 0.02$, $\phi = 0.01$, and $E = 0.2$.

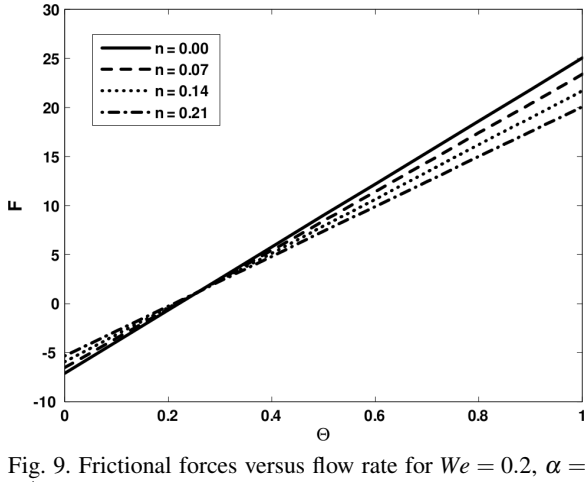

Fig. 9. Frictional forces versus flow rate for $We = 0.2$, $\alpha = \pi/2$, $\phi = 0.05$, and $E = 1$.

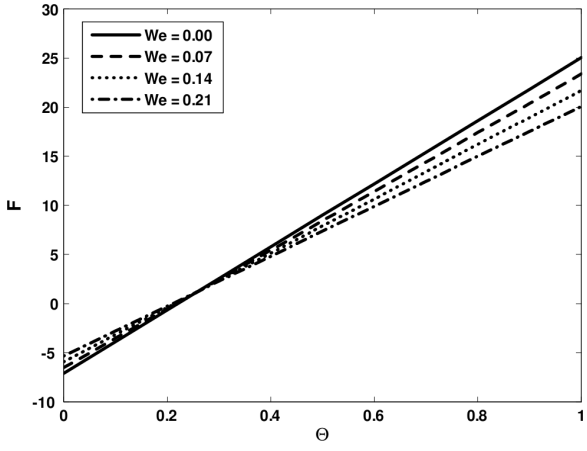

Fig. 10. Frictional forces versus flow rate for $n = 0.05$, $\alpha = \pi/2$, $\phi = 0.05$, and $E = 1$.

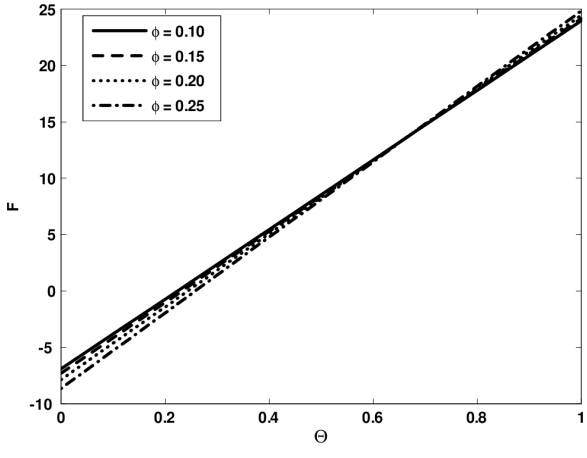

Fig. 11. Frictional forces versus flow rate for $n = 0.05$, $\alpha = \pi/2$, $We = 0.2$, and $E = 1$.

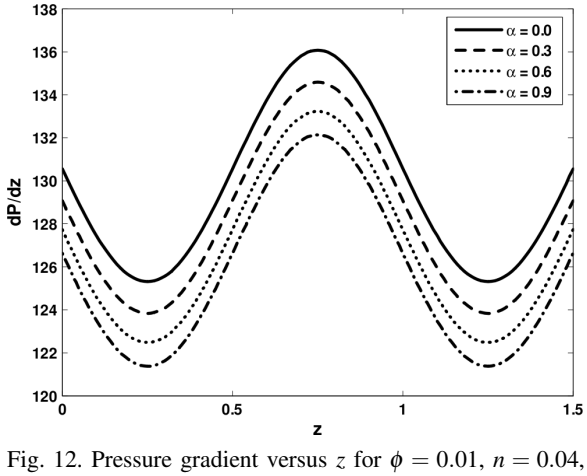

Fig. 12. Pressure gradient versus z for $\phi = 0.01$, $n = 0.04$, $We = 0.1$, $E = 0.3$, and $\Theta = -4$.

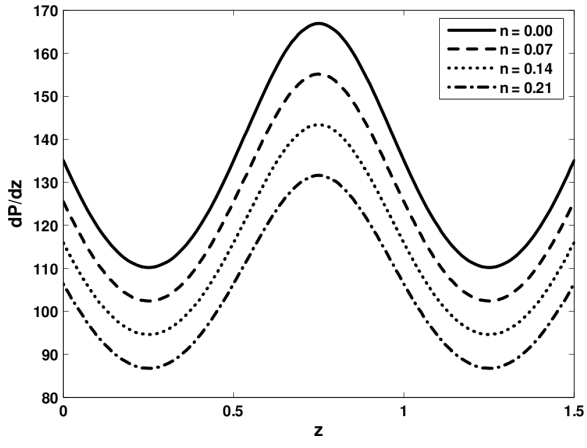

Fig. 13. Pressure gradient versus z for $\phi = 0.05$, $\alpha = \pi/2$, $We = 0.2$, $E = 0.3$, and $\Theta = -4$.

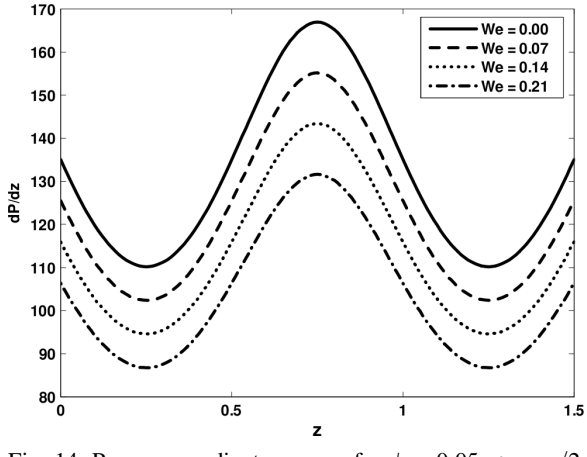

Fig. 14. Pressure gradient versus z for $\phi = 0.05$, $\alpha = \pi/2$, $n = 0.2$, $E = 0.3$, and $\Theta = -4$.

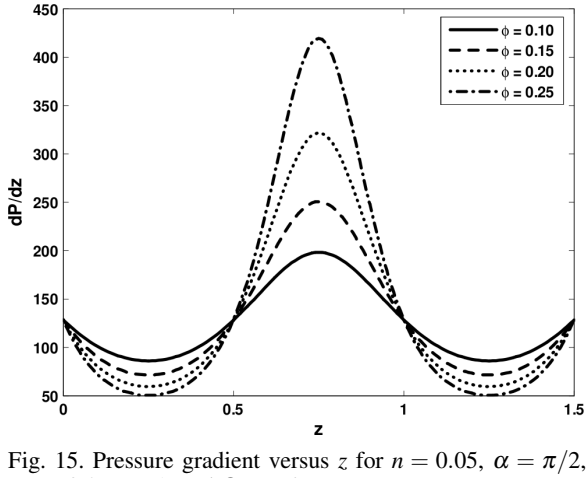

Fig. 15. Pressure gradient versus z for $n = 0.05$, $\alpha = \pi/2$, $We = 0.2$, $E = 1$, and $\Theta = -4$.

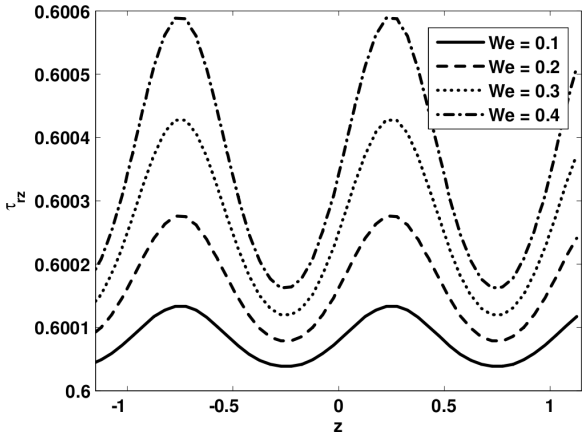

Fig. 16. Shear stress versus z for $n = 0.05$, $\alpha = \pi/2$, $\phi = 0.2$, $E = 1$, and $\Theta = -4$.

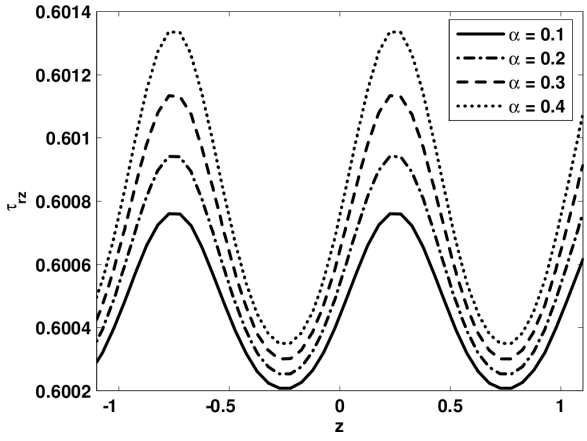

Fig. 17. Shear stress versus z for $n = 0.05$, $We = 0.2$, $\phi = 0.2$, $E = 1$, $\Theta = -4$, and $\alpha = \pi/2$.

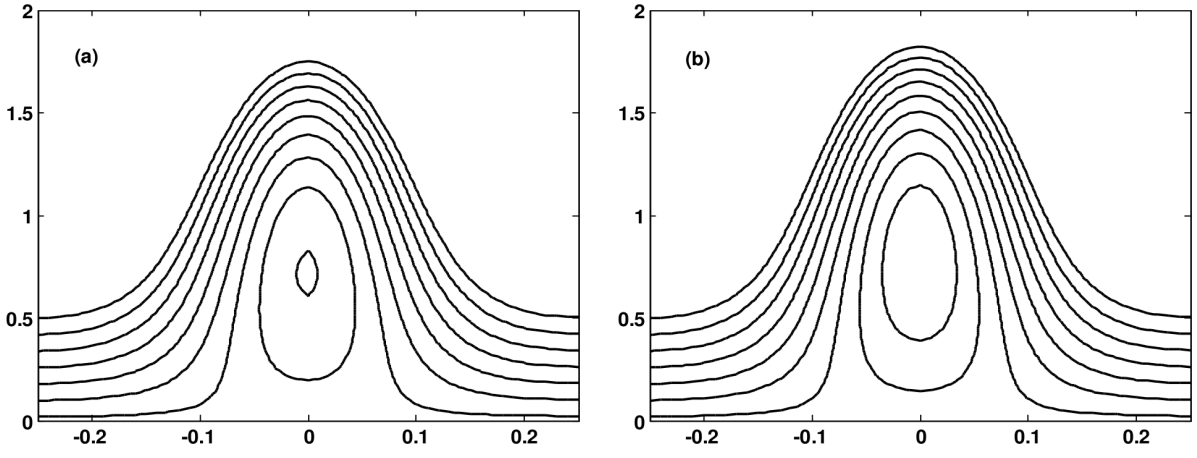

Fig. 18. Streamlines for different values of Θ; (a) $\Theta = 0.1$; (b) $\Theta = 0.2$. The other parameters are $We = 0.1$, $\phi = 0.1$, and $n = 0.02$.

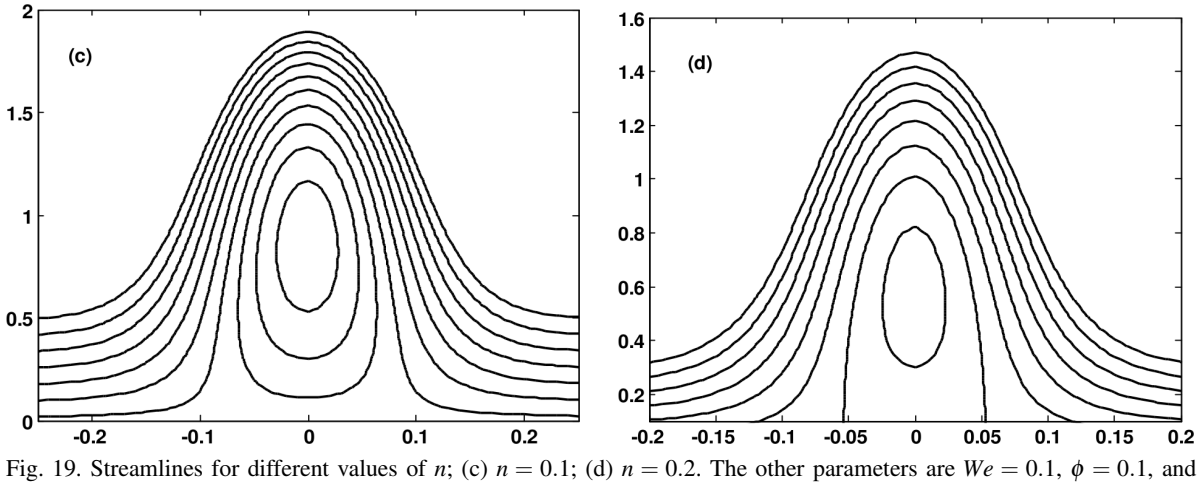

Fig. 19. Streamlines for different values of n; (c) $n = 0.1$; (d) $n = 0.2$. The other parameters are $We = 0.1$, $\phi = 0.1$, and $\Theta = 0.5$.

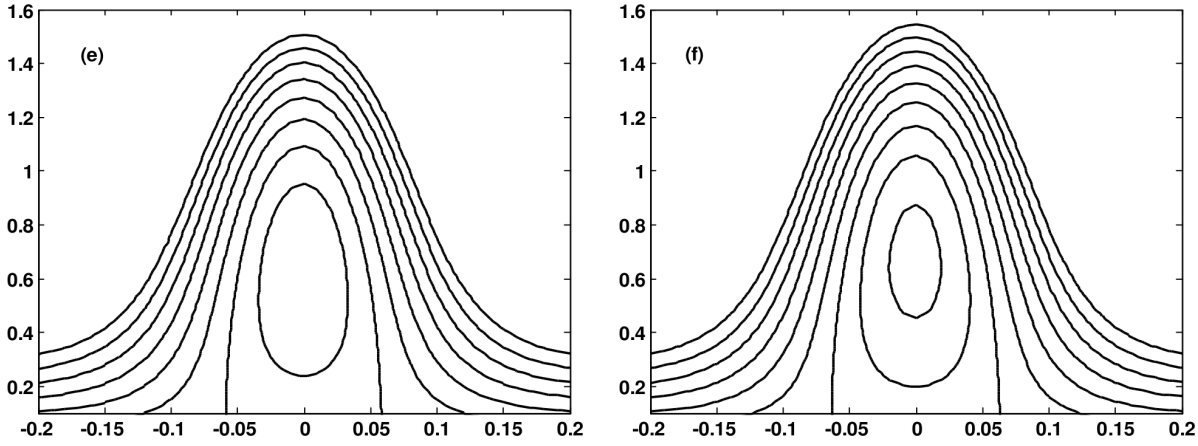

Fig. 20. Streamlines for different values of ϕ; (e) $\phi = 0.1$; (f) $\phi = 0.2$. The other parameters are $We = 0.1$, $n = 0.1$, and $\Theta = 0.5$.

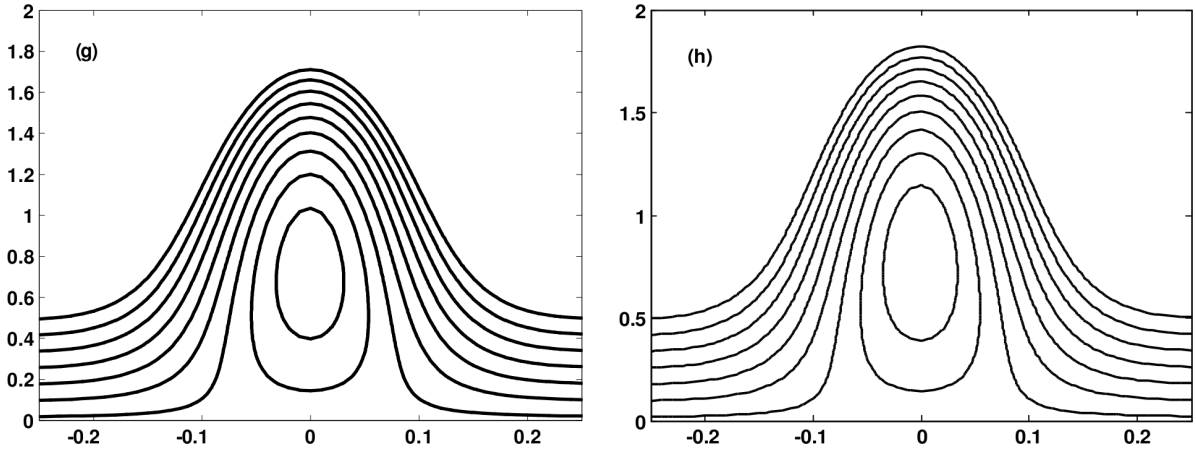

Fig. 21. Streamlines for different values of We; (g) $We = 0.1$; (h) $We = 0.2$. The other parameters are $\phi = 0.1$, $n = 0.1$, and $\Theta = 0.5$.

augmented pumping occurs. Figures 8 to 11 describe the variation of frictional forces. It is seen that frictional forces have opposite behaviour as compared with the pressure rise. Figures 12 to 15 are prepared to see the behaviour of the pressure gradient for different parameters. It is observed that for $z \in [0, 0.5]$ and $[1.1, 1.5]$ the pressure gradient is small, while the pressure gradient is large in the interval $z \in [0.51, 1]$. Moreover, it is seen that an increase in α, n, and We causes the decrease in the pressure gradient, while the pressure gradient increases with the increase in ϕ. Figures 16 and 17 are prepared to see the variation of the shear stress for different values of α and We. It is observed that with an increase in α and We, the shear stress increases. Figure 18 illustrates the streamline graphs for different values of the time mean flow rate Θ. It is observed that when we increase Θ the size of trapped bolus increases. Figure 19 shows the streamlines for different values of (power law index) n. It is analyzed that with the increase in n size and number of trapping bolus decreases. Figure 20 illustrates the streamline graphs for different values of ϕ. It is observed that with the increase in ϕ the trapped bolus increases. The streamlines for different values of We are shown in Figure 21. It is evident from the figure that the size of the trapped bolus increases by increasing We.

Acknowledgement

The authors thank the Higher Education Commission for financial support of this work.

[1] S. Nadeem, Phys. Lett. A **368**, 181 (2007).
[2] S. Nadeem and M. Ali, Commun. Nonlinear Sci. Numer. Simul. **14**, 2073 (2009).
[3] M. Y. Malik, A. Hussain, S. Nadeem, and T. Hayat, Z. Naturforsch. **64a**, 588 (2009).
[4] Kh. S. Mekheimer and Y. Abd Elmaboud, Physica A **387**, 2403 (2008).
[5] S. Nadeem and S. Akram, Z. Naturforsch. **64a**, 713 (2009).
[6] T. Hayat, Y. Wang, A. M. Siddiqui, K. Hutter, and S. Asghar, Math. Models Meth. Appl. Sci. **12**, 1691 (2002).
[7] T. W. Latham, Fluid motion in a peristaltic pump, M. sc, Thesis, Massachusetts Institute of Technology, Cambridge 1966.
[8] T. Hayat and N. Ali, Physica A **370**, 225 (2006).
[9] M. H. Haroun, Commun. Nonlinear Sci. Numer. Simul. **12**, 1464 (2007).
[10] Kh. S. Mekheimer and Y. Abd Elmaboud, Phys. Lett. A **372**, 1657 (2008).
[11] K. Vajravelu, G. Radhakrishnamacharya, and V. Radhakrishnamurty, Int. J. Nonlinear Mech. **42**, 754 (2007).
[12] S. Nadeem, T. Hayat, N. Sher Akbar, and M. Y. Malik, Int. J. Heat Mass Transfer **52**, 4722 (2009).
[13] S. Nadeem and N. Sher Akbar, Commun. Nonlinear Sci. Numer. Simul. **14**, 3844 (2009).
[14] S. Nadeem and N. Sher Akbar, Commun. Nonlinear Sci. Numer. Simul. doi:10.1016/j.cnsns.2009.02.032.
[15] S. Srinivas and M. Kothandapani, Int. Commun. Heat Mass Transf. **35**, 514 (2008).
[16] G. Radhakrishnamacharya and Ch. Srinivasulu, C. R. Mecanique **335**, 369 (2007).
[17] S. Srinivas, R. Gayathria, and M. Kothandapani, Comput. Phys. Commun. **180**, 2115 (2009).
[18] M. Kothandapani and S. Srinivas, Int. J. Nonlinear Mech. **43**, 915 (2008).